catalysts

MDPI

Article

The Catalytic Performance of Nanorod Nickel Catalyst in the Hydrolysis of Lithium Borohydride and Dimethylamine Borane

Meryem Sena Akkus

Department of Energy Systems Engineering, Ankara Yıldırım Beyazıt University, Ankara 06010, Türkiye; msakkus@aybu.edu.tr

Abstract: In the current global energy crisis, the value of hydrogen has become better appreciated. Metal borohydrides attract a lot of attention from researchers because they are rich in hydrogen. In this study, glass microscope slides were coated with nickel as nanorods for use as a catalyst by the magnetron sputtering method, and then catalytic hydrolysis reactions of dimethylamine borane and lithium borohydride were carried out to produce hydrogen. Parameters such as temperature, the amount of catalyst, lithium borohydride, or dimethylamine borane concentration were varied and their effects on the catalytic performances of the catalyst were examined. Moreover, the catalyst was characterized by field emission scanning electron microscopy and X-ray diffraction, and hydrolysis products were analyzed through field emission scanning electron microscopy with energy dispersive spectroscopy analyses. Reaction kinetic parameters were also determined. The activation energy values of dimethylamine borane and lithium borohydride were determined to be 40.0 kJ mol^{-1} and 63.74 kJ mol^{-1}, respectively. Activation enthalpy values were also calculated as 37.34 kJ mol^{-1} and 62.45 kJ mol^{-1} for dimethylamine borane and lithium borohydride, respectively. Initial hydrogen production rates under different conditions were also investigated in the study. For both hydrolysis systems, the fastest hydrogen production rates were calculated as 109 mL $g_{Ni}{}^{-1}$ min^{-1} and 103 mL $g_{Ni}{}^{-1}$ min^{-1} for dimethylamine borane and lithium borohydride, respectively, in the experiment performed at 60 °C at 0.2 M substrate concentration and with 1.3 g of catalyst. These hydrolysis systems using this catalyst are good candidates for systems that need hydrogen.

Keywords: hydrogen; lithium borohydride; dimethylamine borane; nickel; hydrolysis; metal hydride

check for updates

Citation: Akkus, M.S. The Catalytic Performance of Nanorod Nickel Catalyst in the Hydrolysis of Lithium Borohydride and Dimethylamine Borane. *Catalysts* **2023**, *13*, 458. https://doi.org/10.3390/catal13030458

Academic Editors: Loreta Tamasauskaite-Tamasiunaite and Virginija Kepeniene

Received: 4 January 2023
Revised: 8 February 2023
Accepted: 20 February 2023
Published: 22 February 2023

Copyright: © 2023 by the author. Licensee MDPI, Basel, Switzerland. This article is an open access article distributed under the terms and conditions of the Creative Commons Attribution (CC BY) license (https://creativecommons.org/licenses/by/4.0/).

1. Introduction

Polymer Electrolyte Membrane Fuel Cell (PEMFC) technologies have drawn attention in the last years because of their high efficiency and environmental friendliness [1,2]. However, the widespread adoption of PEMFCs has been slow due to various problems associated with the safe and efficient storage of hydrogen [3,4]. There is a need to provide high purity and efficient hydrogen per unit weight without PEMFC poisoning and to develop energy devices that produce hydrogen in appropriate sizes. The above-mentioned requirements greatly limit the choice of hydrogen-producing materials as potential energy carriers. Hydrogen is traditionally stored in gas and liquid form. Storage in compressed gas form contains low hydrogen per unit volume, while high energy consumption and evaporation losses occur when stored in liquefied form [5,6]. It is possible to store hydrogen in solid form in hydrogen-rich borohydrides. The hydrolysis reaction of borohydrides such as $LiBH_4$, $NaBH_4$, NH_3BH_3, $(CH_3)_2NHBH_3$, $LiAlH_4$, etc. is an attractive solution to these problems [7–10]. Of the above compounds, dimethylamine borane ($(CH_3)_2NHBH_3$, DMAB), as one of the NH_3BH_3 derivatives, and lithium borohydride ($LiBH_4$) have attracted attention due to their stability and reversibility, high hydrogen content, etc. [11–14]. Hydrogen can be produced in a controlled manner from the hydrolysis reaction of $LiBH_4$ and DMAB in the presence of proper catalysts [15,16]. The catalytic hydrolysis reactions of $LiBH_4$ and DMAB are given in Equations (1) and (2), respectively. According to Equation (1), 4 mol

of hydrogen is produced from 1 mol of $LiBH_4$, while according to Equation (2), 3 mol of hydrogen is produced from 1 mol of DMAB.

$$LiBH_4 + 2H_2O \xrightarrow{A\ catalyst} LiBO_2 + 4H_2 \quad (1)$$

$$(CH_3)_2NHBH_3 + 2H_2O \xrightarrow{A\ catalyst} [(CH_3)_2NH_2][BO_2] + 3H_2 \quad (2)$$

Many scientists are working on devising catalysts that are easily recyclable, cost-effective, and have good catalytic performance and a high number of reuses for widespread use in catalytic studies. In this context, the first row of the transition metals (vanadium, zinc, copper, nickel, chromium, cobalt, etc.) have the desired properties [17–20]. Among this group of metallic catalysts, especially, there is high catalytic performance, low cost, reusability, etc. Nickel and nickel-composite catalysts attract particular attention because of their important benefits such as catalytic activity, ferromagnetic properties, and reduced operation cost in recycling [21–23].

It is feasible to use nickel as a catalyst in diverse forms such as nanosized materials, foams, thin films, and metal-organic frameworks (MOFs) [24–28]. There are very few studies in the literature in which nickel and its compounds are used as catalysts in the hydrolysis of $LiBH_4$ and DMAB. Liu et. al. (2014) studied hydrogen production by the ball milling of Mg-H_2O and $NiCl_2$ with $LiBH_4$. They calculated the maximum hydrogen production rate as 1655 mL min^{-1} g^{-1} and the yield as 96.1%. The sample composition and grinding time, which are the factors affecting the hydrogen production rate in the planned system, were examined [29]. In another study, the catalytic performance of $CoCl_2$, $NiCl_2$, and $FeCl_3$ in $LiBH_4$ hydrolysis was investigated. Among these chlorides, $CoCl_2$ has faster reaction kinetics. The maximum hydrogen production rate was calculated at 41,701 mL min^{-1} g^{-1} under 5 mL feeding solution, 5% wt. $CoCl_2$ and 40 °C experimental condition [30]. Zhang et al. performed the synthesis of nanosized Pt/$Ni(OH)_2$ catalyst via the immobilization of Pt nanoparticles on $Ni(OH)_2$ colloid and then used this for hydrogen generation from DMAB hydrolysis. It was determined that the prepared catalyst showed 100% hydrogen selectivity. The activation energy value of the Pt/$Ni(OH)_2$-catalyzed DMAB hydrolysis reaction was calculated as 49.94 kJ mol^{-1} by the Arrhenius equation [31]. In another study, Ni particles were first made ready by chemical deposition on hydrophilic polymer nano gel particles and then their performance in DMAB and $NaBH_4$ catalytic hydrolysis was examined. In the kinetic studies, the Arrhenius activation energies of DMAB and $NaBH_4$ were calculated as 50.96 and 47.82 kJ mol^{-1}, respectively [32]. Xu and Liu first reported the effect of alloys of Pt/C with Fe, Co, Ni, and Cu on hydrogen production from DMAB and hydrazine monohydrate. Among them, it was observed that the NiPt/C catalyst had the best catalytic performance. Activation energies were computed as 39.97 and 56.34 kJ mol^{-1} for DMAB hydrolysis using NiPt/C, and Pt/C, respectively [33]. In the study of Cai et al., the kinetic analysis of the catalyst consisting of Ni/Pd nanoclusters dispersed in a polymer hydrogel with a 3D network structure in hydrogen production from the DMAB hydrolysis reaction was performed. The prepared catalyst has an activation energy of 34.95 kJ mol^{-1}. They also stated that the prepared catalyst was long-lived [34]. However, no study was found regarding the use of nanorod-structured nickel catalysts in the hydrolysis of $LiBH_4$ or DMAB. Moreover, there are not enough studies in the literature on the hydrogen generation rate (HGR) of DMAB and $LiBH_4$. In this study, it is thought that the investigation of the HGR values of these compounds' hydrolysis systems using nickel catalysts under different conditions will make an important contribution to the literature. In addition, activation energy, activation enthalpy, and activation entropy values were calculated from the reaction kinetic parameters for both hydrolysis systems.

While investigating catalyst preparation methods, scientists have turned to industrially prepared processes that are inexpensive and have as little a hazardous environmental impact as possible. The main advantages of physical vapor deposition (PVD) techniques, which are an alternative to the chemical synthesis method, are that they are environmen-

tally friendly, do not require toxic precursors, the desired coating is made in one step, and the process is repeatable [35]. Magnetron sputtering, which is one of the PVD techniques, has received a lot of interest in recent years, especially due to its easy industrial application [36]. The thickness of the coatings made with this method can be adjusted, the desired high-quality and uniform coating is achieved with less material; the process is also environmentally friendly and results in the coating of materials with different properties such as hard, corrosion resistant, and optical properties [37,38].

To the best of our knowledge, no study using the glass microscope slide-supported nanorod nickel catalysts for hydrolysis experiments of DMAB and $LiBH_4$ has so far been reported. In this research, a nanorod-structured, porous, and thin-film catalyst was prepared from nickel supported on glass slides by the magnetron sputtering method. In order to examine the catalytic performance of the prepared catalyst in the DMAB and $LiBH_4$ hydrolysis reaction system, parameters such as temperature, DMAB or $LiBH_4$ concentration, and catalyst amount were studied in a wide range. Furthermore, the prepared catalyst's structure was analyzed with field emission scanning electron microscopy (FE-SEM) and X-ray diffraction (XRD), while reaction products were analyzed with field emission scanning electron microscopy with energy dispersive spectroscopy (FE-SEM/EDS).

2. Results and Discussion

2.1. Characterization

X-ray diffractometer (XRD) and field emission scanning electron microscopy (FE-SEM) analyses were performed to determine the structural and morphological properties of the prepared catalysts. The morphology and structure of the prepared nickel catalyst in FE-SEM are demonstrated in Figure 1. The coating thickness was found to be 1100 nm (Figure 1a). Nickel atoms are deposited in the support material in the form of nanorods. Cross-section measurements of the catalyst were also made in different areas. As a result, it was determined that the thickness of the thin-film coating of the catalyst generally showed a homogeneous distribution. The catalyst has a porous structure as seen in Figure 1b. It is seen that the spacing of the nickel rods is not the same everywhere, and in some places, it is quite small.

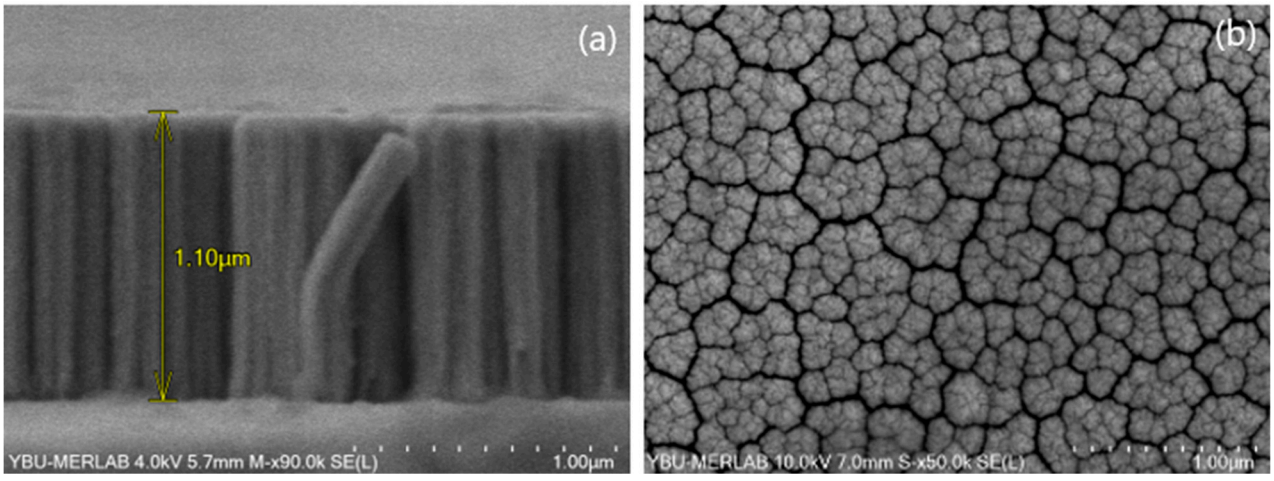

Figure 1. SEM photos of the nickel catalyst (**a**) cross-section, (**b**) planar.

Figure 2 shows the XRD analysis of the catalyst. This demonstrates that the nickel catalyst is in a crystalline structure. Crystal sequences and peaks are found at 44° (111), 52° (200), 76° (220), 93° (311), and 98° (222).

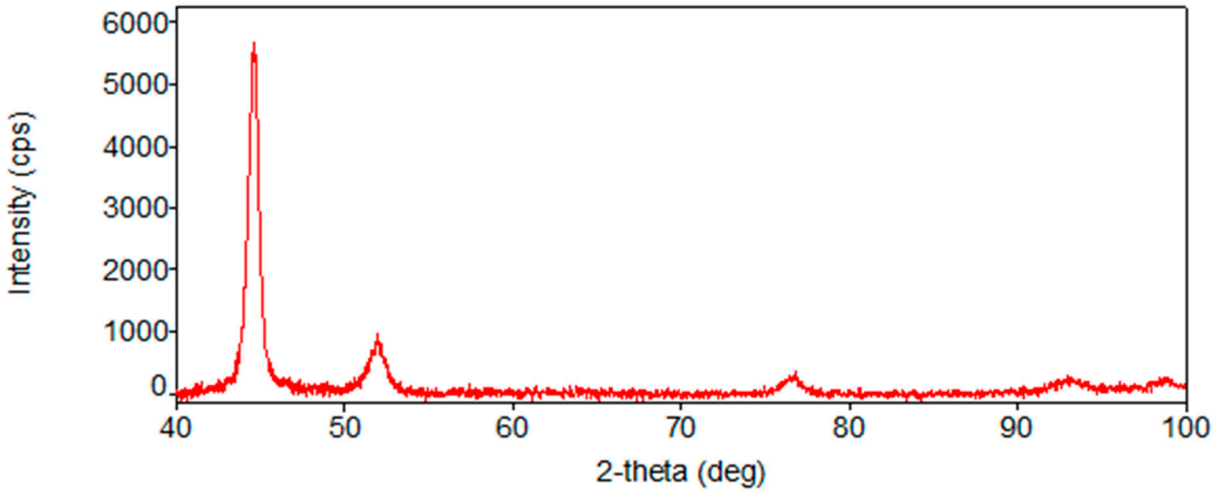

Figure 2. XRD pattern of the nickel catalyst.

The Scherrer formula provides information about the crystal size of the material using XRD data. In the Scherrer formula, given in Equation (3), D_{hkl} denotes crystallinity size, K particle shape factor, λ X-ray wavelength, β_{hkl} half of the peak reflection width, and θ the Bragg angle [39]. Using Equation (3), the crystal size of nickel was calculated as 8 nm.

$$D_{hkl} = \frac{K\,\lambda}{\beta_{hkl}\,cos\theta} \tag{3}$$

FE-SEM/EDS analyses of DMAB and $LiBH_4$ hydrolysis reaction products were performed. Relevant data is given in Figure 3. In general, elemental analyses of the expected products are seen. However, since lithium's atomic energy is very low, the detector could not detect this element. Conversely, the aluminum's peak of the substrate (aluminum foil) is visible from the $LiBH_4$ and DMAB hydrolysis products. This is due to the low concentration of the products. In addition, carbon impurity was observed in the FE-SEM/EDS analysis of the hydrolysis products of $LiBH_4$. It is thought that this impurity may have come from the environment while drying the analysis sample or from the device environment during the SEM analysis. Nickel has not been found in the EDS analyses of both hydrolysis systems. In order to be sure of this situation, different samples were taken from both hydrolysis test systems. SEM/EDS analyses were repeated from different parts of these samples and the result was confirmed. In this case, it was understood that the catalyst prepared for both hydrolysis systems is stable under the hydrolysis conditions.

SEM analyses of the catalyst surface were performed after the fourth reuse from the hydrolysis reactions. Related images are given in Figure 4. It is observed that the by-product accumulates locally on the nickel catalyst surface used in DMAB and $LiBH_4$ hydrolysis experiments. Since the catalyst structure is rod-shaped and nano-porous, it is thought that it is less affected by the accumulation of hydrolysis by-products than a non-porous nickel coating.

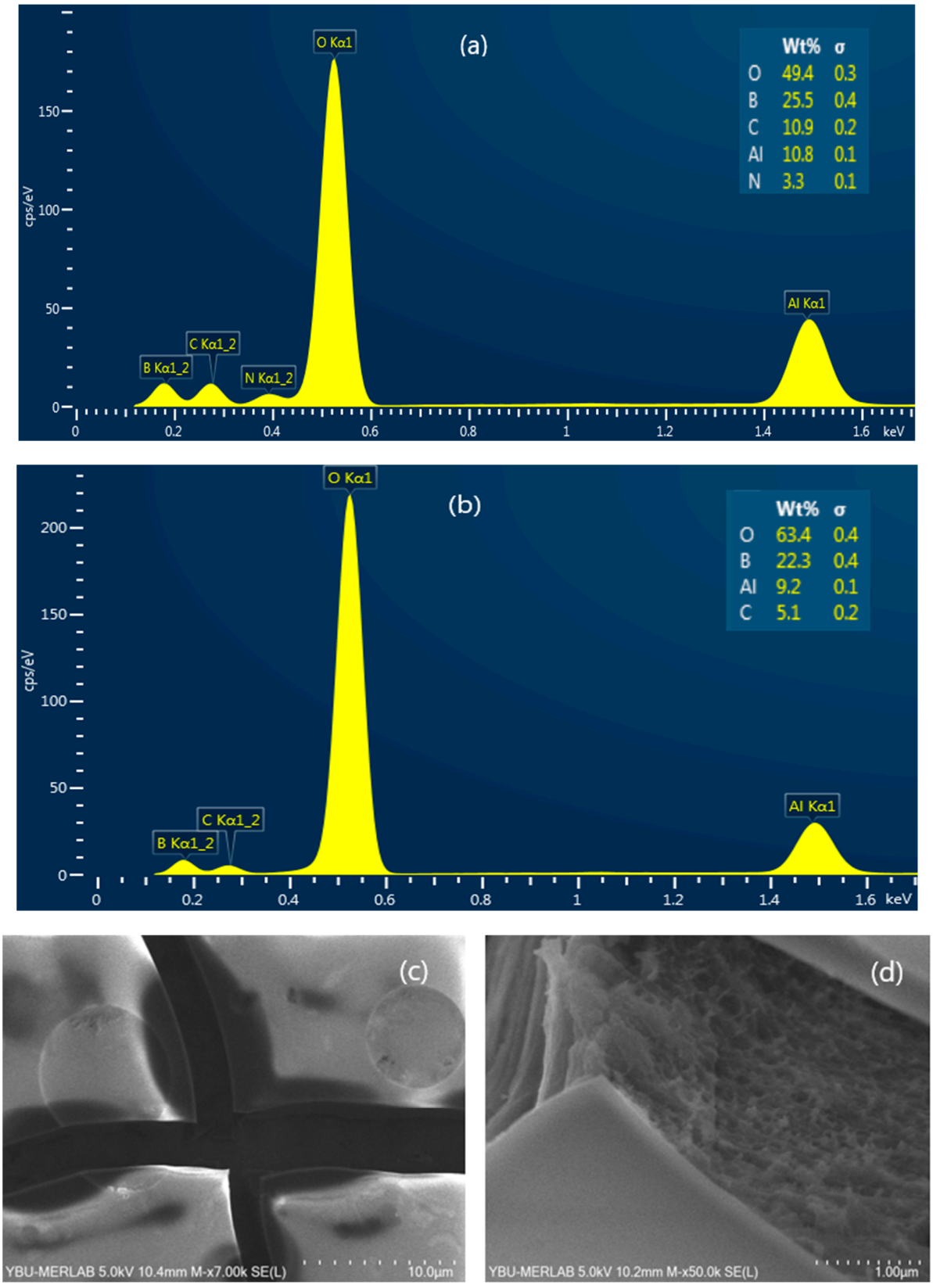

Figure 3. SEM/EDS analysis of DMAB and $LiBH_4$ hydrolysis products. SEM/EDS data for (**a**) DMAB, (**b**) $LiBH_4$, and SEM image for (**c**) DMAB and (**d**) $LiBH_4$.

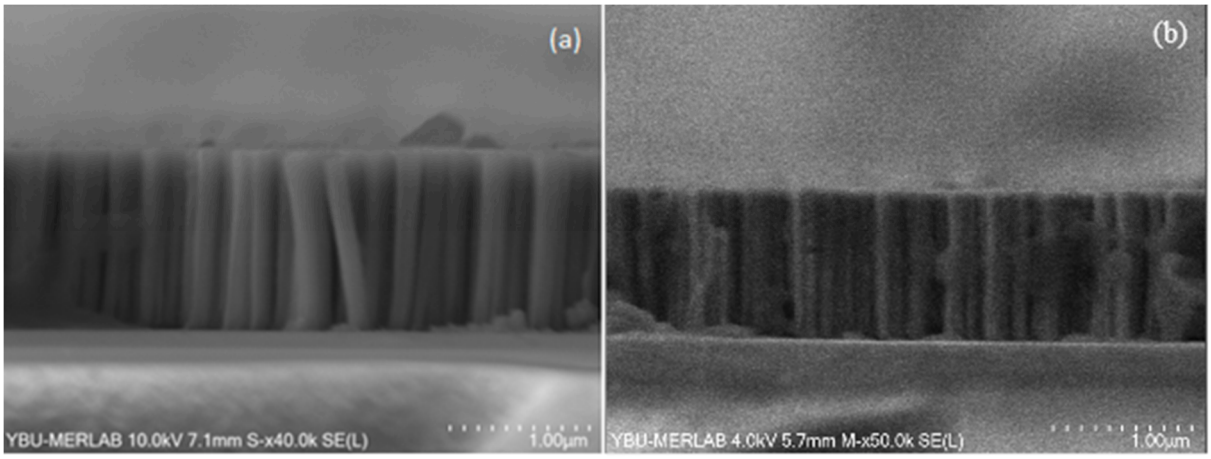

Figure 4. SEM images of catalyst surfaces after the 4th cycle (**a**) catalyst used in DMAB hydrolysis and (**b**) catalyst used in $LiBH_4$ hydrolysis.

2.2. Effect of the Amount of the Nickel Catalyst on Hydrogen Production

The effect of the amount of the nanorod-structured nickel catalyst on H_2 production processes from the hydrolysis reactions of DMAB and $LiBH_4$ was investigated using various amounts of the catalyst, specifically, 1 g, 1.3 g, 1.5 g, and 1.8 g in 0.2 M feeding solution at 40 °C and results are shown in Figure 5. It can be seen that, as the amount of catalyst increases, the reaction time decreases and the volume of H_2 produced increases. In addition, the initial HGR values of both hydrolysis systems increased depending on the amount of catalyst. The HGR values of the DMAB hydrolysis system are 35, 53, 95, and 106 mL g_{Ni}^{-1} min^{-1}, respectively, calculated by increasing the amount of catalyst from 1 g to 1.8 g. The HGR values of the $LiBH_4$ hydrolysis system are 45, 50, 66, and 75 mL g_{Ni}^{-1} min^{-1}, respectively, calculated by increasing the amount of catalyst from 1 g to 1.8 g. The catalyst active sites are capped by the byproducts of the hydrolysis reaction. Therefore, when the amount of catalyst is less, the amount of deactivation is higher.

Additionally, the initial hydrogen generation rates of nanorod-structured nickel-catalyzed DMAB and $LiBH_4$ hydrolysis reactions with different amounts of catalysts were calculated and are given in Table 1.

Table 1. H_2 generation rate with nickel catalyst at different catalyst amounts.

Amount of Catalyst (g)	HGR Value of DMAB (mL g_{cat}^{-1} min^{-1})	HGR Value of $LiBH_4$ (mL g_{cat}^{-1} min^{-1})
1	35	45
1.3	53	50
1.5	95	66
1.8	106	75

The hydrogen production performance of a small amount of nanorod-structured nickel prepared by the sputtering magnetron method as a catalyst is evaluated as good. With this method, it is foreseen that better results will be obtained by making a thicker coating or coating metals that are more active than nickel.

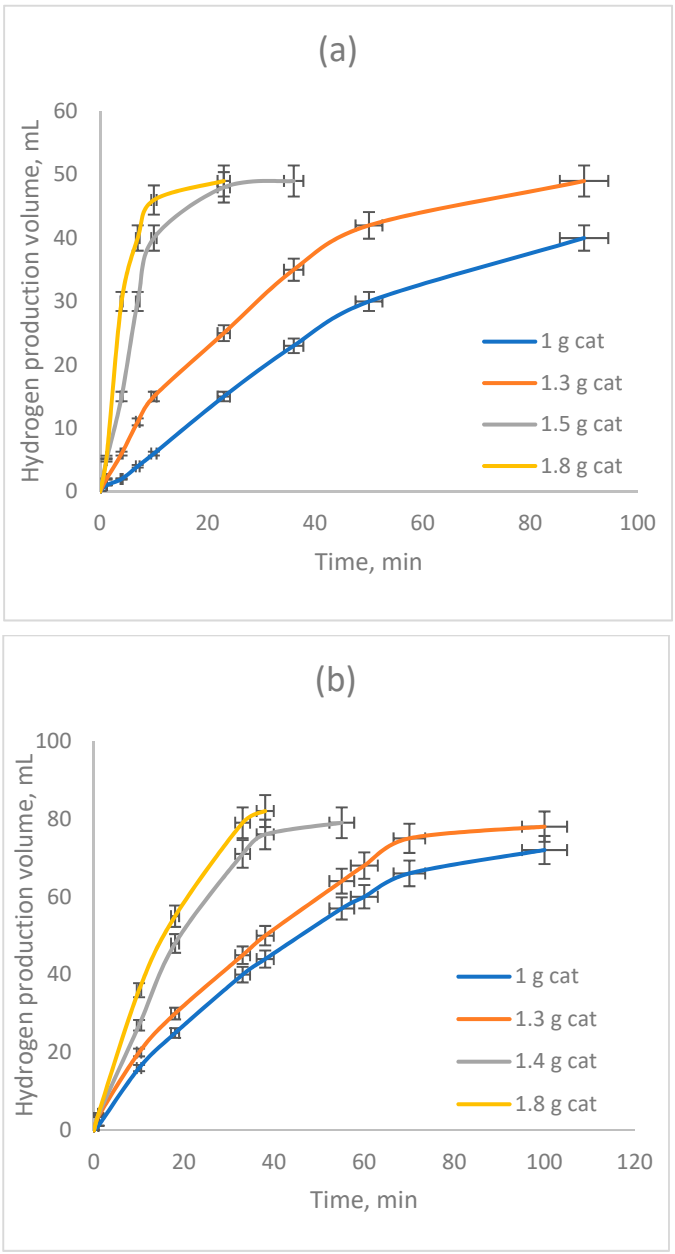

Figure 5. H_2 generation volume versus time over nickel catalyst varied amount of the catalyst. (**a**) DMAB experiments and (**b**) $LiBH_4$ experiments.

2.3. Effect of Substrate Concentration on Hydrogen Generation

The effect of DMAB or $LiBH_4$ concentration on the hydrolysis processes were investigated with various initial concentration of substrate, specifically, 0.025 M, 0.05 M, 0.1 M, and 0.2 M solution, 1.3 g catalyst at 40 °C. The plots of the generated hydrogen volume versus time are shown in Figure 6. It can be seen that the reaction time and the amount of hydrogen produced both increase as the substrate concentration increases. It is observed that HGR values increased as $LiBH_4$ concentration decreased. However, the reaction rate in DMAB in two dilute solutions was lower than in other concentrated solutions. The reason for this is interpreted as the fact that DMAB molecules are less in number than in water, so mass transfer towards the catalyst is intense. Therefore, the contact surfaces with the catalyst are less.

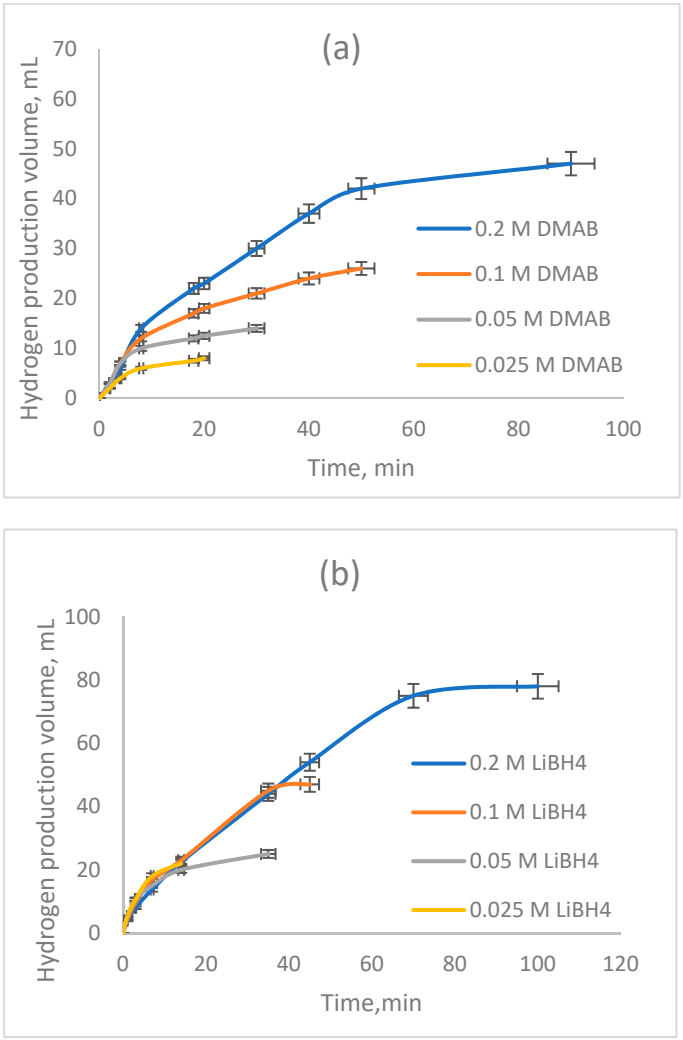

Figure 6. Plots of produced hydrogen volumes versus time for H_2 generation upon hydrolysis process under various initial concentrations of (**a**) DMAB experiments and (**b**) $LiBH_4$ experiments.

HGR values calculated against each initial substrate concentration are given in Table 2.

Table 2. HGR values with nickel catalyst at different substrate concentrations.

Substrate Concentration (M)	HGR Value of DMAB (mL g_{cat}^{-1} min^{-1})	HGR Value of $LiBH_4$ (mL g_{cat}^{-1} min^{-1})
0.2	54	50
0.1	53	76
0.05	45	93
0.025	43	100

2.4. Effect of Temperature of the Nickel Catalyst on Hydrogen Generation

The reaction temperature effects on the hydrolysis process catalyzed by nanorod-structured nickel catalysts were studied at 30 °C, 40 °C, 50 °C, and 60 °C, with 0.2 M DMAB or 0.2 M $LiBH_4$ and 1.3 g catalyst. Figure 7 shows the plots of the produced hydrogen volume versus time. It can be seen that the hydrogen production time is reduced by increasing the reaction temperature from 30 °C to 60 °C.

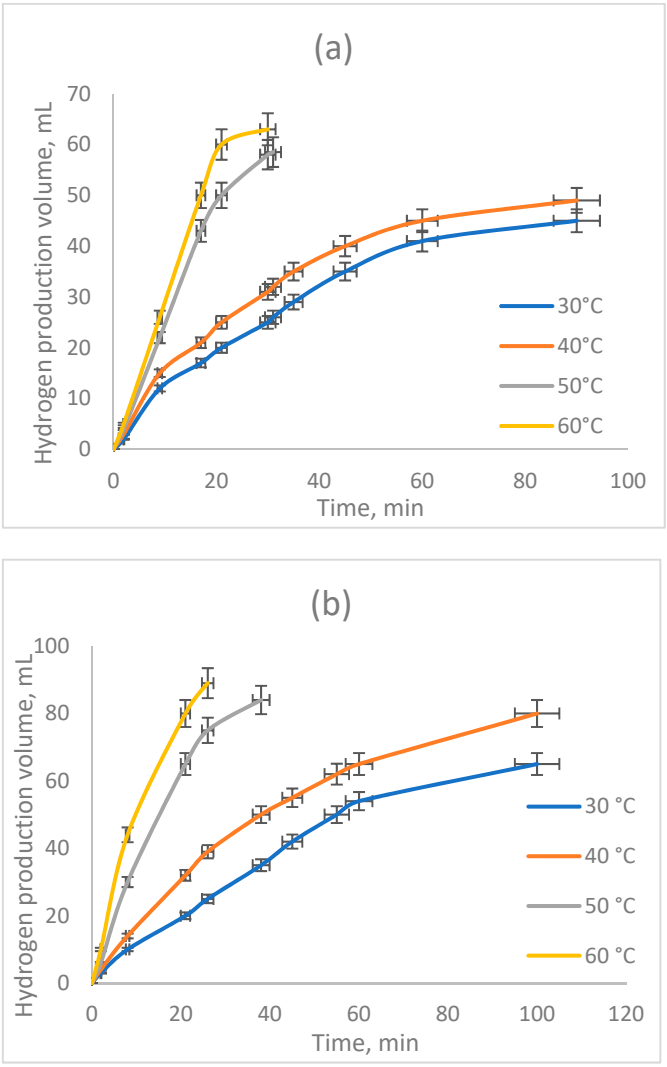

Figure 7. Plots of the effect of temperature on the produced hydrogen volume versus time. (**a**) DMAB graph and (**b**) $LiBH_4$ graph.

HGR values calculated against each temperature are given in Table 3. The highest HGR value for the DMAB system was calculated as 109 mL $g_{Ni}{}^{-1}$ min^{-1} at 60 °C, while the lowest HGR value was calculated as 34 mL $g_{Ni}{}^{-1}$ min^{-1} at 30 °C. Hydrolysis of DMAB appears to be an endothermic reaction [31]. In the $LiBH_4$ system, the lowest and highest HGR values were calculated as 31 mL $g_{Ni}{}^{-1}$ min^{-1} and 103 mL $g_{Ni}{}^{-1}$ min^{-1} at 30 °C and 60 °C, respectively.

Table 3. HGR values with nickel catalyst at different temperatures.

Temperature (°C)	HGR Value of DMAB (mL $g_{cat}{}^{-1}$ min^{-1})	HGR Value of $LiBH_4$ (mL $g_{cat}{}^{-1}$ min^{-1})
30	34	31
40	80	50
50	90	100
60	109	103

The activation parameters for the catalytic hydrolysis process of DMAB and $LiBH_4$ were also calculated by the Arrhenius and Eyring equations (Figures 8 and 9, respectively). In order to determine the activation energy, the graphs of the reaction were plotted as zero-, first-, and second-order for each hydrolysis experiment, and R^2 values were deduced. In

the experiments, the highest R^2 values were observed in the first-order reaction. Figure 8 shows graphs of $1/T$ vs. lnk. The activation energy (E_a) values of DMAB and $LiBH_4$ were calculated to be 40.0 kJ mol^{-1} and 63.74 kJ mol^{-1}, respectively. The activation energy values calculated from the hydrolysis studies of DMAB and $LiBH_4$ with nickel were similar to the literature.

The E_a value of $LiBH_4$ was higher than the E_a value of DMAB. The reason for this is the strong ionic and covalent bonds in the $LiBH_4$ structure; the bonding configurations also increase the activation energies. As a result, it is observed that hydrogen release occurs slowly [9].

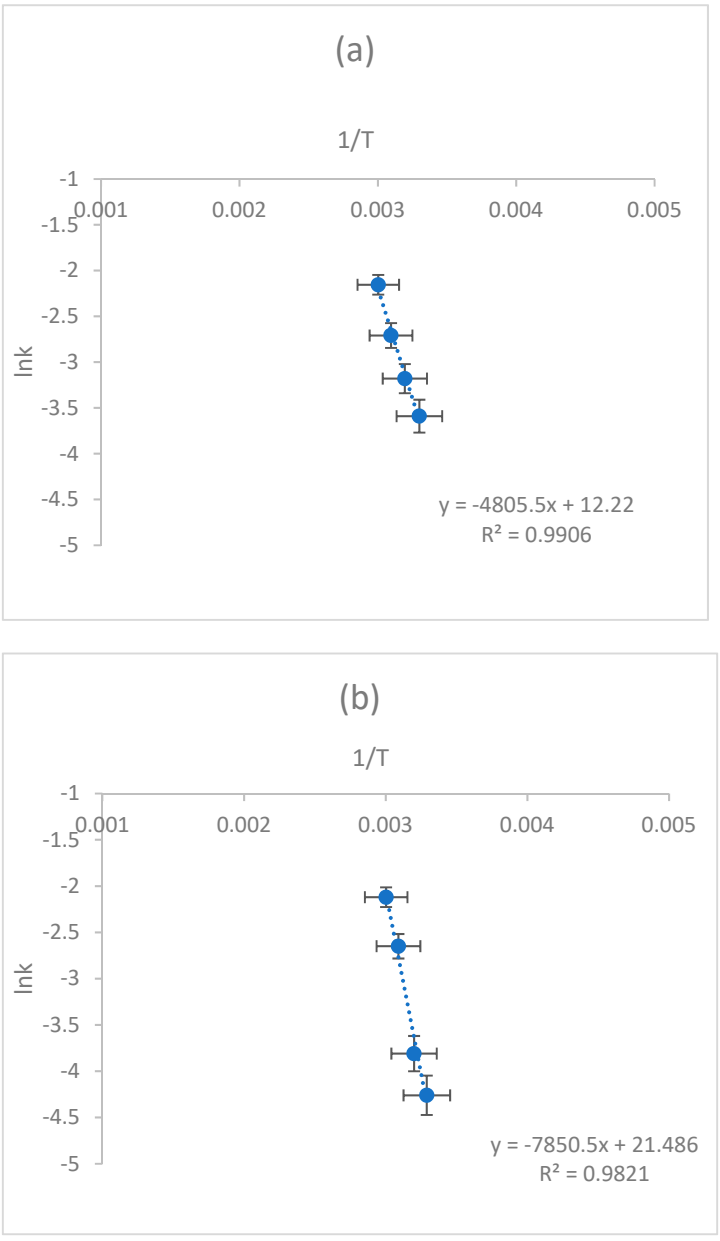

Figure 8. The graph of $1/T$ versus lnk. (**a**) DMAB graph and (**b**) $LiBH_4$ graph.

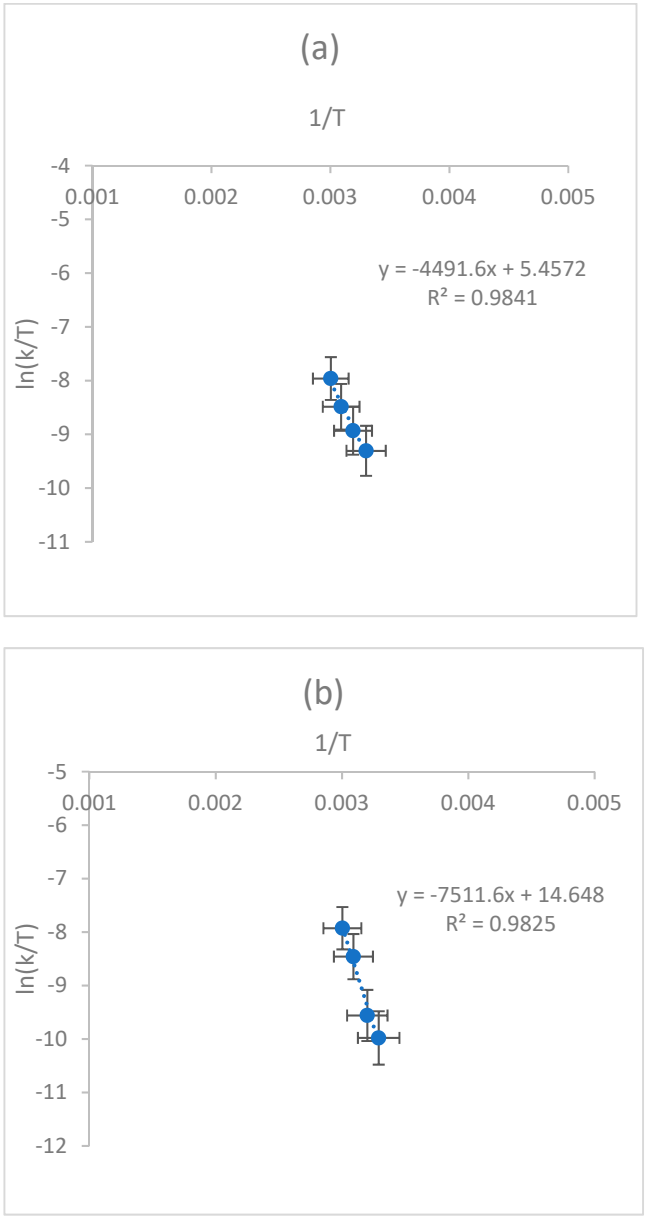

Figure 9. The graph of $1/T$ versus ln(k/T). (**a**) DMAB graph and (**b**) $LiBH_4$ graph.

The Eyring equation is given in Equation (4). $1/T$ versus In(k/T) was plotted and the activation enthalpy ($\Delta H^{\#}$) and activation entropy ($\Delta S^{\#}$) were calculated (Figure 7) [40]. In Equation (4), T is the temperature in Kelvin, R is the gas constant (8.314 J $mol^{-1}K^{-1}$), k is the rate, h is the Planck constant (6.63 $\times$ 10^{-34} J·s), k_B is the Boltzmann constant (1.38 $\times$ 10^{-23} J·K^{-1}), $\Delta S^{\#}$ is the activation entropy is, and $\Delta H^{\#}$ is the activation enthalpy. For DMAB, $\Delta S^{\#}$ is -152 J mol^{-1} K^{-1} and $\Delta H^{\#}$ is 37.34 kJ mol^{-1}. For $LiBH_4$, $\Delta S^{\#}$ is -75.74 J mol^{-1} K^{-1} and $\Delta H^{\#}$ is 62.45 kJ mol^{-1}. Negative activation entropies are considered to show that the total number of molecules decreases in the hydrolysis rate-determining step of the elementary reaction and that the reaction proceeds through an associative mechanism that may include the participation of the water molecule on the reactant substrate in the rate-determining step [34].

$$\ln \frac{k}{T} = -\frac{\Delta H^{\#}}{R} \frac{1}{T} + \ln \frac{k_B}{h} + \frac{\Delta S^{\#}}{R} \quad (4)$$

2.5. Investigation of the Reusability of the Catalyst

The reusability of the prepared catalyst was investigated. The catalyst used in the experiment was washed with deionized water and dried after each cycle, making it ready for the next reuse. Catalyst repeatability test conditions for both catalytic test systems were performed at 0.2 M substrate concentration, 1.8 g catalyst, and 50 °C. The cycle was repeated four times (Figure 10). The prepared nickel catalyst showed several cycles of reusability performance in the hydrolysis of DMAB and $LiBH_4$, and a conversion of around 80% was achieved in the fourth cycle in both hydrolysis reactions. The reason for the decrease in the performance of the catalyst is the accumulation of side product material on the active surfaces of the catalysts. It is thought that the use of dilute solution and the porous catalyst structure contribute positively to the conversion for reuse. Catalysts can be treated with a dilute acid solution between reuses, thus improving the reuse performance of the catalyst.

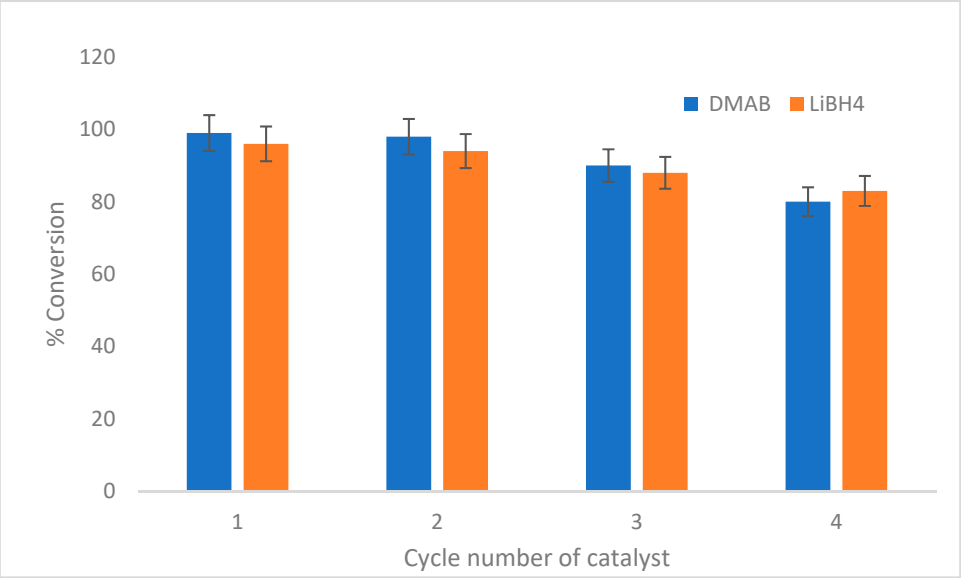

Figure 10. The reusability of nickel catalysts for DMAB and $LiBH_4$ hydrolysis for four cycles.

3. Materials and Methods

3.1. Preparation of Nanorod Nickel Catalyst

A microscope slide was preferred as catalyst support material. The reason for using the slides is that the activity of nickel is better observed and the slides are easy to obtain and use. The selected slides were Isolab brand, 26 mm × 76 mm in size, and of non-running flat glass. For a homogeneous surface in catalyst preparation, first, the slides must be cleaned. For this, slides were kept for 15 min at 50 °C in organic solutions of acetone, isopropyl alcohol, and ethanol, respectively. Acetone and isopropyl alcohol from Isolab (Eschau, Germany) of 99.5% purity were used, while the ethanol was from Sigma-Aldrich (St. Louis, MO, USA) and of 99.5% purity. Next, the slides were washed with distilled water. The cleaned slides were left to dry at 80 °C. Finally, they were cut into 1 cm × 1.5 cm sizes before coating.

The nickel sputtering target was supplied by Nanografi (Ankara, Turkey), and had a diameter and thickness of 2" and 0.125", respectively. The purity of the nickel target was 99.99%. An Optosense high vacuum magnetron plasma sputtering device was used to make the coatings. The magnetron sputtering conditions were as follows. In RF mode, 150 W sputtering power was used, the coating medium was filled with high purity argon gas (99.999%, Linde), the ambient pressure was 0.07 mbar, the distance between the target and slides was 10 cm, and the coating time was 100 min.

3.2. Hydrolysis Experiments

The materials used in catalytic hydrolysis experiments to produce hydrogen were $LiBH_4$ (Sigma-Aldrich, St. Louis, MO, USA, 95% purity) and Borane dimethylamine complex (Sigma-Aldrich, St. Louis, MO, USA, 97% purity). The thickness of the catalysts used in the reactions was the same. However, the slides were cut according to the desired amount of catalyst and added to a heat-resistant glass reactor. The reactor was placed in a water bath so that the temperature of the reactor was homogeneous. While feeding, a specially designed pressure-compensating liquid feeding apparatus with a volume of 15 mL was used. The volume of the feeding solution (DMAB or $LiBH_4$) was 4 mL. The experimental plan of the hydrolysis experiments was as follows. The planned quantity of catalyst was placed at the two-neck reactor and the temperature of the rector and the water bath were allowed to equalize. While the reactant solutions were fed from the first neck of the reactor, a 500 mL gas burette (custom manufacturing from heat-resistant glass) was attached to quantify the H_2 volume released from the other neck. In the hydrolysis experiments, the stopwatch was started when the feeding was done. The volume of hydrogen produced was measured against time in the gas burette system. The initial hydrogen generation rate (HGR) value is computed from the proportion of the gradient of the graph of the produced hydrogen volume versus duration at a linear regime rate to the quantity of coated catalyst.

3.3. Characterization

The structural property of the nanorod-structured nickel catalyst was examined using a Rigaku Miniflex 600 Tabletop Powder X-ray diffractometer (Rigaku, Tokyo, Japan). Operational conditions were 40 kV, 0.02-degree scan steps, and 15 mA. The system had a CuKα source with λ = 0.1546 nm. The scan range was from 40 to 100 degrees. The analysis time was 30 min. In addition, the Bragg–Brentano (BB) Geometry method was used in the XRD analysis of the samples.

The morphology and structure of nickel catalysts were determined using field emission scanning electron microscopy (Hitachi, high-vacuum FE-SEM SU5000, Tokyo, Japan). 4 or 10 kV was used to optimize the resolution of the images. Elemental analyses of the substances in the solutions were carried out after the hydrolysis reactions of DMAB and $LiBH_4$. For this analysis, 0.5 mL of hydrolysis product solutions were taken and self-dried on aluminum foil. These materials were then analyzed by field emission scanning electron microscopy with energy dispersive spectroscopy (FE-SEM/EDS) analysis. The EDS Detector was an Oxford X-Max N80 (Oxford Instruments, Abingdon, UK) with a detector area of 80 mm^2.

4. Conclusions

In this study, nickel thin film catalysts consisting of nanorods were prepared on glass microscope slides by the magnetron sputtering method. The thickness of the thin film was 1100 nm. These prepared catalysts were used in DMAB and $LiBH_4$ hydrolysis experiments. The factors affecting the performance of the catalytic hydrolysis reactions such as temperature, catalyst amount, and DMAB or $LiBH_4$ concentration were studied. The results showed that the hydrolysis reactions of DMAB and $LiBH_4$ fit first-order kinetics. The activation energy values of DMAB and $LiBH_4$ were calculated to be 40.0 kJ mol^{-1} and 63.74 kJ mol^{-1}, respectively. Activation entropy values were calculated as -152 J mol^{-1} K^{-1} and -75.74 J mol^{-1} K^{-1} for DMAB and $LiBH_4$, and activation enthalpy values were calculated as 37.34 kJ mol^{-1} and 62.45 kJ mol^{-1} for DMAB and $LiBH_4$, respectively. As a conclusion of this study, nanorod-structured nickel-catalyzed DMAB and $LiBH_4$ hydrolysis reaction systems are seen as good candidates to generate hydrogen.

Funding: This research was funded by Ankara Yıldırım Beyazıt University Scientific Research Unit grant number 2148.

Data Availability Statement: The data presented in this study are available on request from the corresponding author.

Conflicts of Interest: The author declares no competing financial interest.

References

1. Wang, Y.; Diaz, D.F.R.; Chen, K.S.; Wang, Z.; Adroher, X.C. Materials, technological status, and fundamentals of PEM fuel cells—A review. *Mater. Today* **2020**, *32*, 178–203. [CrossRef]
2. Kallem, P.; Yanar, N.; Choi, H. Nanofiber-based proton exchange membranes: Development of aligned electrospun nanofibers for polymer electrolyte fuel cell applications. *ACS Sustain. Chem. Eng.* **2018**, *7*, 1808–1825. [CrossRef]
3. Dai, P.; Zhao, X.; Xu, D.; Wang, C.; Tao, X.; Liu, X. Preparation, characterization, and properties of Pt/Al_2O_3/cordierite monolith catalyst for hydrogen generation from hydrolysis of sodium borohydride in a flow reactor. *Int. J. Hydrogen Energy* **2019**, *44*, 28463–28470. [CrossRef]
4. Krishnan, P.; Hsueh, K.L.; Yim, S.D. Catalysts for the hydrolysis of aqueous borohydride solutions to produce hydrogen for PEM fuel cells. *Appl. Catal. B Environ.* **2007**, *77*, 206–214. [CrossRef]
5. Simagina, V.I.; Ozerova, A.M.; Komova, O.V.; Netskina, O.V. Recent advances in applications of Co-B catalysts in $NaBH_4$-based portable hydrogen generators. *Catalysts* **2021**, *11*, 268. [CrossRef]
6. Zheng, J.; Liu, X.; Xu, P.; Liu, P.; Zhao, Y.; Yang, J. Development of high pressure gaseous hydrogen storage technologies. *Int. J. Hydrogen Energy* **2012**, *37*, 1048–1057. [CrossRef]
7. Wang, C.; Wang, Q.; Fu, F.; Astruc, D. Hydrogen generation upon nanocatalyzed hydrolysis of hydrogen-rich boron derivatives: Recent developments. *Acc. Chem. Res.* **2020**, *53*, 2483–2493. [CrossRef] [PubMed]
8. Ouyang, L.; Liu, M.; Chen, K.; Liu, J.; Wang, H.; Zhu, M. Recent progress on hydrogen generation from the hydrolysis of light metals and hydrides. *J. Alloys Compd.* **2022**, *910*, 164831. [CrossRef]
9. Li, C.; Peng, P.; Zhou, D.W.; Wan, L. Research progress in $LiBH_4$ for hydrogen storage: A review. *Int. J. Hydrogen Energy* **2011**, *36*, 14512–14526. [CrossRef]
10. Usman, M.R. Hydrogen storage methods: Review and current status. *Renew. Sustain. Energy Rev.* **2022**, *167*, 112743. [CrossRef]
11. Pal, P.; Kumari, P.; Wang, Y.; Isobe, S.; Kumar, M.; Ichikawa, T. Destabilization of $LiBH_4$ by the infusion of Bi_2X_3 (X = S, Se, Te): An in situ TEM investigation. *J. Mater. Chem. A* **2020**, *8*, 25706–25715. [CrossRef]
12. Mauron, P.; Buchter, F.; Friedrichs, O.; Remhof, A.; Bielmann, M.; Zwicky, C.N. Stability and reversibility of $LiBH_4$. *J. Phys. Chem. B* **2008**, *112*, 906–910. [CrossRef]
13. Luo, Y.; Sun, L.; Xu, F.; Liu, Z. Improved hydrogen storage of LiBH4 and NH_3BH_3 by catalysts. *J. Mater. Chem. A* **2018**, *6*, 7293–7309. [CrossRef]
14. Li, S.; Miao, P.; Zhang, Y.; Wu, J.; Zhang, B.; Du, Y. Recent advances in plasmonic nanostructures for enhanced photocatalysis and electrocatalysis. *Adv. Mater.* **2021**, *33*, 2000086. [CrossRef]
15. Tunç, N.; Rakap, M. Surfactant-aided synthesis of RhCo nanoclusters as highly effective and recyclable catalysts for the hydrolysis of methylamine borane and dimethylamine borane. *Catal. Sci. Technol.* **2020**, *10*, 7865–7874. [CrossRef]
16. Karatas, Y.; Acidereli, H.; Gulcan, M.; Sen, F. A novel highly active and reusable carbon based platinum-ruthenium nanocatalyst for dimethylamine-borane dehydrogenation in water at room conditions. *Sci. Rep.* **2020**, *10*, 1–10. [CrossRef] [PubMed]
17. Loghmani, M.H.; Shojaei, A.F.; Khakzad, M. Hydrogen generation as a clean energy through hydrolysis of sodium borohydride over Cu-Fe-B nano powders: Effect of polymers and surfactants. *Energy* **2017**, *126*, 830–840. [CrossRef]
18. Yu, Y.; Kang, L.; Sun, L.; Xu, F.; Pan, H.; Sang, Z. Bimetallic Pt-Ni nanoparticles confined in porous titanium oxide cage for hydrogen generation from NaBH4 hydrolysis. *Nanomaterials* **2022**, *12*, 2550. [CrossRef]
19. Xu, D.; Zhang, X.; Zhao, X.; Dai, P.; Wang, C.; Gao, J. Stability and kinetic studies of MOF-derived carbon-confined ultrafine Co catalyst for sodium borohydride hydrolysis. *Int. J. Energy Res.* **2019**, *43*, 3702–3710. [CrossRef]
20. Xu, D.; Wang, H.; Guo, Q.; Ji, S. Catalytic behavior of carbon supported Ni–B, Co–B and Co–Ni–B in hydrogen generation by hydrolysis of KBH_4. *Fuel Process. Technol.* **2011**, *92*, 1606–1610. [CrossRef]
21. Lu, Z.H.; Li, J.; Feng, G.; Yao, Q.; Zhang, F.; Zhou, R. Synergistic catalysis of MCM-41 immobilized Cu–Ni nanoparticles in hydrolytic dehydrogeneration of ammonia borane. *Int. J. Hydrogen Energy* **2014**, *39*, 13389–13395. [CrossRef]
22. Ji, Z.; Shen, X.; Zhu, G.; Zhou, H.; Yuan, A. Reduced graphene oxide/nickel nanocomposites: Facile synthesis, magnetic and catalytic properties. *J. Mater. Chem.* **2012**, *22*, 3471–3477. [CrossRef]
23. Liu, C.H.; Chen, B.H.; Hsueh, C.L.; Ku, J.R.; Jeng, M.S.; Tsau, F. Hydrogen generation from hydrolysis of sodium borohydride using Ni–Ru nanocomposite as catalysts. *Int. J. Hydrogen Energy* **2009**, *34*, 2153–2163. [CrossRef]
24. Lai, Q.; Aguey-Zinsou, K.F.; Demirci, U.B. Nanosizing ammonia borane with nickel–An all-solid and all-in-one approach for H2 generation by hydrolysis. *Int. J. Hydrogen Energy* **2018**, *43*, 14498–14506. [CrossRef]
25. Zhao, Y.; Jiao, L.; Liu, Y.; Guo, L.; Li, L.; Liu, H. A synergistic effect between nanoconfinement of carbon aerogels and catalysis of CoNiB nanoparticles on dehydrogenation of $LiBH_4$. *Int. J. Hydrogen Energy* **2014**, *39*, 917–926. [CrossRef]
26. Yousef, A.; Barakat, N.A.; El-Newehy, M.; Kim, H.Y. Chemically stable electrospun NiCu nanorods@ carbon nanofibers for highly efficient dehydrogenation of ammonia borane. *Int. J. Hydrogen Energy* **2012**, *37*, 17715–17723. [CrossRef]

27. Yousef, A.; Barakat, N.A.; Khalil, K.A.; Unnithan, A.R.; Panthi, G.; Pant, B. Photocatalytic release of hydrogen from ammonia borane-complex using Ni (0)-doped TiO_2/C electrospun nanofibers. *Colloids Surf. A Physicochem. Eng. Asp.* **2012**, *410*, 59–65. [CrossRef]
28. Yang, J.; Zheng, C.; Xiong, P.; Li, Y.; Wei, M. Zn-doped Ni-MOF material with a high supercapacitive performance. *J. Mater. Chem. A* **2014**, *2*, 19005–19010. [CrossRef]
29. Liu, Y.; Wang, X.; Liu, H.; Dong, Z.; Cao, G.; Yan, M. Exploration of hydrogen generation from an Mg–$LiBH_4$ system improved by NiCl2 addition. *J. Power Sources* **2014**, *251*, 459–465. [CrossRef]
30. Chen, K.; Ouyang, L.; Wang, H.; Liu, J.; Shao, H.; Zhu, M. A high-performance hydrogen generation system: Hydrolysis of LiBH4-based materials catalyzed by transition metal chlorides. *Renew Energy* **2020**, *156*, 655–664. [CrossRef]
31. Zhang, Q.; Xu, F.; Huang, W.; Wang, Y.; Liu, X. Hydrogen production upon the hydrolysis of dimethylamineborane over Pt/Ni $(OH)_2$ nanocomposite. *Fuel* **2022**, *324*, 124695. [CrossRef]
32. Cai, H.; Liu, L.; Chen, Q.; Lu, P.; Dong, J. Ni-polymer nanogel hybrid particles: A new strategy for hydrogen production from the hydrolysis of dimethylamine-borane and sodium borohydride. *Energy* **2016**, *99*, 129–135. [CrossRef]
33. Xu, F.; Liu, X. Synergistically promoted H2 evolution from dimethylamine-borane and hydrazine monohydrate by simply alloying of Pt/C with Ni. *Fuel* **2021**, *304*, 121433. [CrossRef]
34. Cai, H.K.; Jiang, Z.Y.; Xu, S.; Xu, Y.; Lu, P.; Dong, J. Polymer Hydrogel Supported Ni/Pd Alloys for Hydrogen Gas Production from Hydrolysis of Dimethylamine Borane with a Long Recyclable Lifetime. *Polymers* **2022**, *14*, 4647. [CrossRef] [PubMed]
35. Arzac, G.; Fernández, A. Advances in the implementation of PVD-based techniques for the preparation of metal catalysts for the hydrolysis of sodium borohydride. *Int. J. Hydrogen Energy* **2020**, *45*, 33288–33309. [CrossRef]
36. Fu, K.; Zeng, L.; Liu, J.; Liu, M.; Li, S.; Guo, W. Magnetron sputtering a high-performance catalyst for ultra-low-Pt loading PEMFCs. *J. Alloys Compd.* **2020**, *815*, 152374. [CrossRef]
37. Kelly, P.J.; Arnell, R.D. Magnetron sputtering: A review of recent developments and applications. *Vacuum* **2000**, *56*, 159–172. [CrossRef]
38. Regmi, G.; Velumani, S. Radio frequency (RF) sputtered ZrO2-ZnO-TiO_2 coating: An example of multifunctional benefits for thin film solar cells on the flexible substrate. *Sol. Energy* **2023**, *249*, 301–311. [CrossRef]
39. Bokuniaeva, A.O.; Vorokh, A.S. Estimation of particle size using the Debye equation and the Scherrer formula for polyphasic TiO_2 powder. *J. Phys. Conf. Ser.* **2019**, *1410*, 012057. [CrossRef]
40. Niranjan, K. Phase and reaction equilibrium, and phase transitions. In *Engineering Principles for Food Process and Product Realization*; Springer: Berlin/Heidelberg, Germany, 2022; pp. 125–143.

Disclaimer/Publisher's Note: The statements, opinions and data contained in all publications are solely those of the individual author(s) and contributor(s) and not of MDPI and/or the editor(s). MDPI and/or the editor(s) disclaim responsibility for any injury to people or property resulting from any ideas, methods, instructions or products referred to in the content.